Global Biogeochemical Cycles

RESEARCH ARTICLE
10.1029/2019GB006379

Key Points:
- We observed spatial variations of δ^{66}Zn in the deep water of the NWPO and found considerably lighter δ^{66}Zn than the NEPO
- The sedimentary input may be a major cause of relatively light dissolved δ^{66}Zn in the deep water of the NWPO
- Aerosol Zn input is a major cause of the variations of [Zn] and δ^{66}Zn in the surface water of the NWPO

Supporting Information:
- Supporting Information S1

Correspondence to:
T.-Y. Ho,
tyho@gate.sinica.edu.tw

Citation:
Liao, W.-H., Takano, S., Yang, S.-C., Huang, K.-F., Sohrin, Y., & Ho, T.-Y. (2020). Zn isotope composition in the water column of the Northwestern Pacific Ocean: The importance of external sources. *Global Biogeochemical Cycles*, *34*, e2019GB006379. https://doi.org/10.1029/2019GB006379

Received 24 JUL 2019
Accepted 17 DEC 2019
Accepted article online 9 JAN 2020

Zn Isotope Composition in the Water Column of the Northwestern Pacific Ocean: The Importance of External Sources

Wen-Hsuan Liao[1], Shotaro Takano[2], Shun-Chung Yang[1,3], Kuo-Fang Huang[4], Yoshiki Sohrin[2], and Tung-Yuan Ho[1,5]

[1]Research Center for Environmental Changes, Academia Sinica, Taipei, Taiwan, [2]Institute for Chemical Research, Kyoto University, Uji, Japan, [3]Department of Earth Sciences, University of Southern California, Los Angeles, CA, USA, [4]Institute of Earth Sciences, Academia Sinica, Taipei, Taiwan, [5]Institute of Oceanography, National Taiwan University, Taipei, Taiwan

Abstract We determined Zn isotope composition (δ^{66}Zn) in the water column of the Northwestern Pacific Ocean (NWPO) and its marginal seas to investigate the processes driving vertical and spatial variations. Comparable to previous studies, dissolved δ^{66}Zn was relatively low in the top 200 m, ranging from −0.91 to +0.24‰ and increased with depth toward an averaged value, +0.38±0.10‰, in deep water. We found that δ^{66}Zn observed in the deep water of the NWPO was much lower than the Northeastern Pacific Ocean. Box model approaches suggest that spatial variations in the deep water may be attributed to isotopically light Zn originating from sedimentary input or anthropogenic aerosols. In the surface water, the fractionation factors derived from both closed or open system fractionation models are all less than one in the NWPO. However, both closed and open system models show a relatively poor fit to the measured data. We thus propose that external input is a major factor causing the variations of [Zn] and δ^{66}Zn values in surface water, in addition to the effects of scavenging, physical mixing, and biological uptake. As elevated [Zn] and relatively light δ^{66}Zn in the surface water were observed in high aerosol input regions, aerosol deposition may play a dominant role in regulating Zn elemental and isotopic composition in the surface ocean.

1. Introduction

Trace metal concentrations and their isotope composition can serve as useful tracers and proxies for studying material cycling in the ocean (Anderson & Henderson, 2005). Zinc (Zn), an essential micronutrient for the growth of many marine phytoplankton groups, exhibits a nutrient type vertical profile closely correlating with silicate concentrations (Bruland, 1980; Bruland et al., 1978). The puzzling correlation between dissolved Zn and silicate has drawn the attention of oceanographers to study its internal cycling processes in the marine water column. As the vertical profiles of dissolved Zn concentrations ([Zn]) are spatially similar, the distribution pattern of [Zn] alone provides limited information on its cycling processes. Spatial distribution patterns of Zn isotope composition (δ^{66}Zn) would provide further insights in understanding its sources, sinks, and internal cycling processes in marine water column (Moynier et al., 2017). Recent studies on dissolved δ^{66}Zn have provided further insight for Zn cycling in different oceanic regions, including the North Atlantic Ocean (Conway & John, 2014), the Southern Ocean (SO; Zhao et al., 2014; Sieber et al., 2019; Wang et al., 2019), the Southeastern Pacific Ocean (SEPO; John et al., 2017), and the Pacific Ocean (Bermin et al., 2006; Conway & John, 2015; John & Conway, 2014; Samanta et al., 2017; Vance et al., 2019). Several mechanisms have been proposed to explain the distribution of dissolved Zn elemental and isotopic composition in marine water column globally. Scavenging has been first proposed to be a dominant process for its isotopic distribution (John & Conway, 2014). A recent large-scale study in Atlantic Ocean has demonstrated the dominant role of physical mixing on the distribution of dissolved Zn concentrations (Middag et al., 2019). The "SO hypothesis" suggests the importance of biological uptake on global Zn distribution in addition to the effect of physical mixing (de Souza et al., 2018; Vance et al., 2017).

Most of the studies mentioned above found that δ^{66}Zn is relatively low in oceanic surface water and homogeneous in deep water. The isotopic composition can be expressed by δ^{66}Zn as defined in equation (1).

$$\delta^{66}Zn = \left[\left(^{66}Zn/^{64}Zn\right)_{sample}/\left(^{66}Zn/^{64}Zn\right)_{standard\ (JMC-Lyon)} - 1\right] \times 10^3 \quad (1)$$

Global seawater δ^{66}Zn values at depths deeper than 1,000 m seem to be relatively constrained, with an average value of +0.47±0.15‰ from a compilation of about 700 data points from the studies mentioned above. The major cause for the constrained value of δ^{66}Zn in deep water has been attributed to physical processes (Conway & John, 2014). Despite the general homogeneity of δ^{66}Zn in deep water, some studies indicate that the δ^{66}Zn values in deep water may shift due to external sources, such as sedimentary and hydrothermal inputs. Deviations of up to 0.20‰ were observed in the deep water of the Atlantic Ocean and the eastern tropical Pacific Ocean (Conway & John, 2014; John et al., 2017). It is known that sedimentary input can be a major source for dissolved Fe in intermediate and deep water of the subarctic region of the Northwestern Pacific Ocean (NWPO; Nishioka et al., 2007; Nishioka et al., 2013). Sedimentary input originating from the continental margin may also elevate Zn concentrations in the North Pacific Intermediate Water (Conway & John, 2015). In addition to sedimentary input, anthropogenic aerosol deposition can be a dominant Zn source in the surface ocean, especially in regions with high aerosol deposition (Chester & Jickells, 2012; Nriagu & Pacyna, 1988; Pacyna & Pacyna, 2001). Our previous studies have demonstrated that anthropogenic aerosols are the dominant source of Zn and some other particulate trace metals in the surface and deep waters of the NWPO and its marginal seas (Ho et al., 2007; Liao et al., 2017; Liao & Ho, 2018). The inputs of anthropogenic aerosols and sedimentary materials are potentially important processes influencing the spatial distribution of [Zn] and δ^{66}Zn in the water column of the NWPO. An understanding of δ^{66}Zn would illuminate the importance of these external sources in the water column.

In the surface ocean, previous studies observed relatively low dissolved δ^{66}Zn in almost all of the major oceanic regions with the exception of the SO. In the surface water of the SO, dissolved δ^{66}Zn is comparable to or slightly isotopically heavier than the values observed in the deep water (Sieber et al., 2019; Wang et al., 2019; Zhao et al., 2014). A recent study in the subarctic Northeastern Pacific Ocean also observed some isotopically heavy signal in the surface water (Vance et al., 2019). The low dissolved δ^{66}Zn observations are apparently at odds with the expectation that isotopically light Zn would be preferentially taken up by phytoplankton, leaving behind heavy Zn in dissolved pool. Actually, culture experiments have observed that phytoplankton take up isotopically light Zn relative to the culture medium, with 0.2 to 0.4‰ difference between phytoplankton and the medium (John et al., 2007; Köbberich & Vance, 2017, 2018; Samanta et al., 2018). However, recent studies have argued that Zn fractionation of biological uptake can be insignificant due to the complexation effect of organic ligands in culture medium. Marković et al. (2017) observed that organic ligand complexed Zn is isotopically heavy relative to inorganic Zn and the difference is comparable to the one observed between phytoplankton and bulk culture medium. Moreover, two other studies suggested that some phytoplankton may preferentially take up heavy Zn, particularly under Fe limiting condition (Köbberich & Vance, 2017, 2019).

On the other hand, some studies have demonstrated that adsorption of Zn onto degrading phytoplankton or biofilms tends to remove relatively heavy Zn from seawater (Coutaud et al., 2014; John et al., 2007; John & Conway, 2014). Köbberich and Vance (2018) found that bulk biomass δ^{66}Zn were isotopically heavy under high Fe availability, which can be attributed to partial Zn adsorption onto surface-bound Fe-hydroxides. We also found that Zn to P ratios in suspended particles were an order of magnitude higher than the intracellular range for phytoplankton in oceanic regions strongly influenced by anthropogenic aerosol deposition, which reinforces the notion of scavenging of anthropogenic aerosol Zn onto plankton cell surfaces (Ho et al., 2007; Liao & Ho, 2018). Modeling studies also support the importance of scavenging on Zn cycling in the global ocean (Roshan et al., 2018; Weber et al., 2018). Scavenging is thus considered as one of the major processes determining Zn isotope composition in the surface water.

In the North Pacific Ocean (NPO), although quite a few studies have reported spatial [Zn] distribution (Jakuba et al., 2012; Janssen & Cullen, 2015; Kim et al., 2015; Kim et al., 2017; Lohan et al., 2002; Martin et al., 1989), concentration alone cannot identify the relative importance of the various processes mentioned above. To further investigate the influence of internal cycling processes and external sources on Zn cycling in the NWPO, we determined both δ^{66}Zn and [Zn] in the water column of nine sampling stations covering four oceanic regions of the NWPO, including the South China Sea (SCS), the Western Philippine Sea (WPS), the

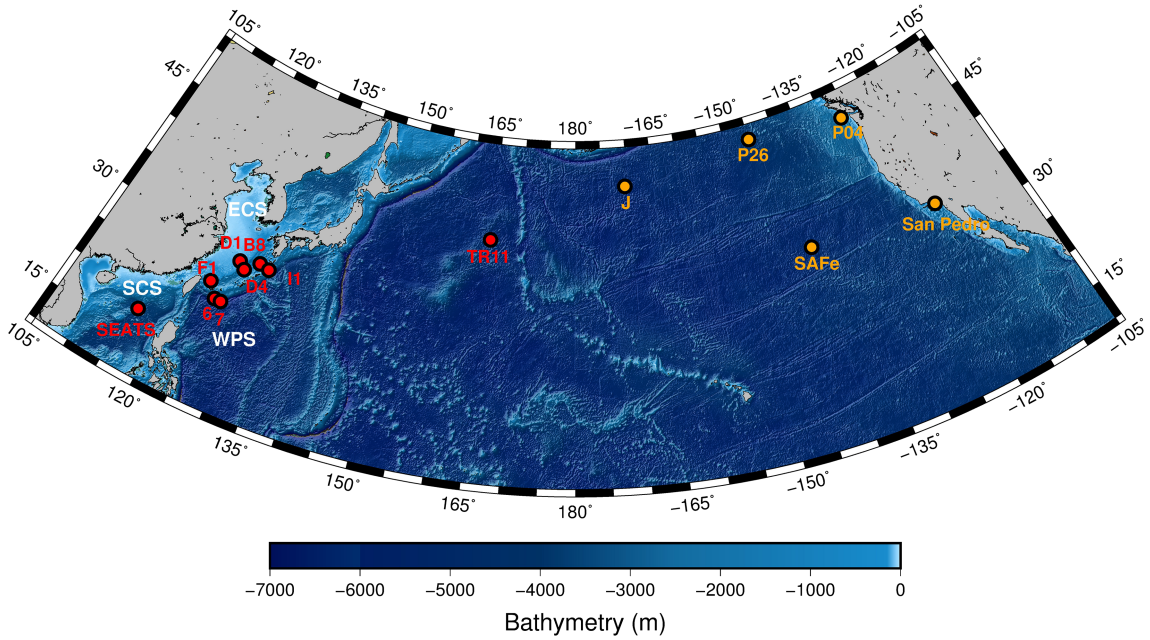

Figure 1. Locations of sampling stations in this study (red circles) and stations from the literature (orange circles) in the North Pacific Ocean (Station J: John and Conway (2014); P04 and P26: Bermin et al. (2006) and Vance et al. (2019); SAFe and San Pedro: Conway and John (2015)).

Kuroshio region adjacent to the East China Sea (ECS), and the Kuroshio extension region (Figure 1), particularly focusing on evaluating the impact of external source inputs on Zn cycling in the NWPO.

2. Materials and Methods

2.1. Sampling and Pretreatment

Seawater samples were collected from five cruises carried out by three research vessels (Figure 1). Seawater samples from the SCS were collected at the South East Asia Time-series Study (SEATS) station by R/V Ocean Researcher I during OR1-812 cruise (October 2006), samples from the NWPO were collected at station TR11 by R/V Hakuho Maru during KH-11-7 cruise (July 2011), samples from the WPS were collected by R/V Ocean Researcher V during OR5-1307-3 and OR5-0035 Taiwan GEOTRACES cruises (station 7 in July 2013 and station 6 in March 2014), and samples from the ECS were collected by R/V Hakuho-maru during KH-15-3 cruise (B8, F1, D1, D4, and I1, October 2015). All seawater samples were collected with acid-cleaned Teflon coated Go-Flo bottles on Taiwanese vessels OR1 and OR5 and X-type Niskin bottles on the Japanese vessel Hakuho Maru. The analytical methods and the data of hydrographic parameters and major nutrients are presented in Figures S1 to S3 in the supporting information. For trace metal analysis, seawater was filtered onboard through in-line 0.22-μm acid-cleaned Polycap cartridge filters (Whatman) or 0.2-μm capsule filters (Acropak, Pall Co.). The samples were then stored in acid-cleaned 500 ml or 1-L low-density polyethylene bottles (Nalgene), which were rinsed with filtered seawater 3 times prior to sampling. Seawater samples were subsequently acidified to pH 1.8 with ultrapure HCl (Seastar or J. T. Baker) then stored until further processing.

δ^{66}Zn analysis was carried out by double spike technique. Detailed technical procedures are described in Conway et al. (2013) and Takano et al. (2017). In brief, approximately 1 L of seawater was used for δ^{66}Zn analysis for samples collected at depths where the [Zn] are relatively high. Two liters of seawater were used for samples collected at depths shallower than 200 m. Before isotopic analysis, [Zn] were determined to calculate the amount of double spike solution needed. Using NOBIAS Chelate-PA 1 resin, the pretreatment procedures for [Zn] analysis were modified from the studies of Sohrin et al. (2008) and Wang et al. (2014). The detailed procedures are described in Table S1 in the supporting information. Calculated with the determined [Zn] information, the double spike solution of ^{67}Zn-^{70}Zn was added to seawater samples with sample-to-spike mass ratio of 1:1 (Rudge et al., 2009). ^{67}Zn-^{70}Zn spike can optimize the isotopic analysis with limited

seawater sample volume (John, 2012). It is suggested that the composition with 48.31% ^{67}Zn and 51.69% ^{70}Zn may yield lowest error for Zn isotope measurement (Rudge et al. (2009). The Zn isotope composition of our ^{67}Zn-^{70}Zn spike solution contained 0.63% ^{64}Zn, 1.06% ^{66}Zn, 49.47% ^{67}Zn, and 48.83% ^{70}Zn, which is close to the proposed ratio with lowest error. Concentrated double spike solution was purified by AG-MP1 resin to remove other trace metal impurities by the procedure described in the following paragraph. The concentrations of our double spike solution were validated by isotopic dilution method with accurately weighted international standard, NIST-683.

Adding double spike solution to the seawater samples, we then carried out the preconcentration step by using NOBIAS Chelate-PA 1 resin to separate trace metals from major salts (Table S1). Zn was further extracted and separated from the eluted preconcentrated trace metals by using anion exchange column filled with AG MP-1M resins. After the elemental separation, the samples were evaporated to dryness and refluxed with 0.5-ml concentrated ultrapure HNO_3 overnight then evaporated to dryness again. Subsequently, 0.05 N ultrapure HNO_3 was added to the dried samples for final redissolution to achieve a working sample concentration level of around 100 ppb. The detailed procedures are described in Table S1, which was modified from Takano et al. (2017).

2.2. Determination of [Zn] and δ^{66}Zn

All of the δ^{66}Zn measurements were conducted using Neptune Plus multi-collector inductively coupled plasma mass spectrometry (Thermo Fisher Scientific) with a PFA integrated nebulizer (100 μl/min; Elemental Scientific) and Apex-IR (Elemental Scientific) introduction system at the Institute of Earth Sciences, Academia Sinica. Normal Ni sampler and X-type skimmer cones were used to acquire high sensitivity of Zn. Cup setting and instrumental settings of the Neptune Plus are listed in Table S2. δ^{66}Zn was measured under medium resolution with a typical ^{64}Zn sensitivity, 0.1 V/ppb. The signal voltages were measured on the left flat shoulder of the combined metal-argide peak, based on the technique of Weyer and Schwieters (2003). Solutions of pure standard (NIST-683), pure spike, and mixtures of three different sample-to-spike ratios (4 to 1, 1 to 1, and 1 to 4) were analyzed for data reduction at the beginning of each analytical batch. Stable isotopic ratios were calculated from an average of 30 cycles using a data reduction scheme based on the approach of Siebert et al. (2001). The isotopic ratios of each sample were obtained from the averaged value of duplicate analyses. A standard-sample bracketing method was also used in this study to monitor the instrument condition during the analysis. Mixtures of standard (NIST-683) and spike were designed to match [Zn] and sample-to-spike ratio of samples and were used to bracket every five samples. δ^{66}Zn are expressed in per mil (‰) relative to NIST-683 using delta notation as described in equation (1). The internal error of each sample (2σ) was calculated by the propagated 1σ error for each individual analysis with two bracketing standards (Conway et al., 2013). The theoretical source of errors in isotopic composition analysis by double spike technique includes errors from counting statistics, Johnson noise, and isobaric interference (Conway et al., 2013; John, 2012). Our measured errors matched well with the theoretical error calculated from Monte Carlo simulation (John, 2012; Figure S4), showing reliable external accuracy.

Traditionally, δ^{66}Zn are expressed relative to Lyon JMC Zinc (JMC-3-0749-Lyon). Compared to NIST-683, the δ^{66}Zn of Lyon JMC Zn we observed was -0.15±0.03‰ (n = 10), which is indistinguishable from previously published values, −0.12±0.04‰ (Chen et al., 2016). We thus used +0.12‰ as the correction factor for all of the obtained isotopic values based on NIST-683 to Lyon JMC Zn by equation (2). The δ^{66}Zn expressed in this study were all relative to Lyon JMC Zinc (JMC-3-0749-Lyon).

$$\delta^{66}Zn_{JMC-Lyon} = \left[\left(^{66}Zn/^{64}Zn\right)_{sample}/\left(^{66}Zn/^{64}Zn\right)_{NIST-683} - 1\right] \times 10^3 + \delta^{66}Zn_{NIST-683\ to\ JMC-Lyon} \quad (2)$$

Comparable to values reported in Takano et al. (2017), Ni blanks for PA1 extraction and Zn purification were 0.15 and 0.04 ng, respectively. We also monitored ^{62}Ni during isotopic analysis to correct the interference from ^{64}Ni on ^{64}Zn. The signals of ^{64}Ni, calculated from ^{62}Ni, in the samples were generally 4 orders of magnitude lower than ^{64}Zn signal. Thus, the interference of ^{64}Ni on ^{64}Zn is negligible.

With the information of isotope ratios obtained, the known sample volume, and the spike volume, [Zn] in samples was calculated by using an isotope dilution approach.

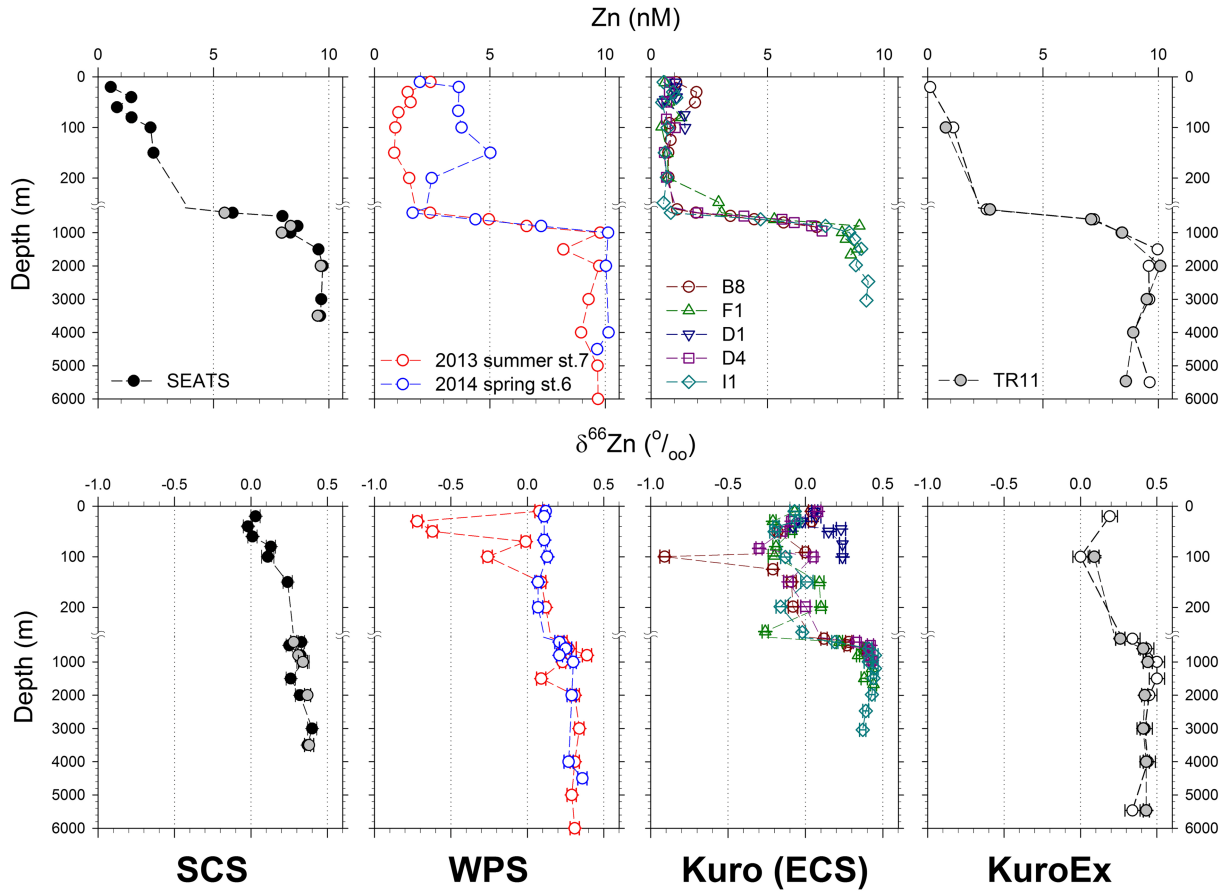

Figure 2. Zn concentrations and isotope composition in the water column of the studied sites. Gray circles shown in the SEATS and TR11 profiles represent the intercomparison results. The relative standard deviation of Zn concentration analysis was around 9% (Table S3). The error bars of δ^{66}Zn data represent internal analytical error (2σ).

2.3. Accuracy Validation

We have determined three international Zn isotope standards, IRMM-3702, ETH AA, and NIST-682, and the δ^{66}Zn we obtained are +0.27±0.05 (n > 200), +0.26±0.03 (n = 10), and −2.44±0.02‰ (n = 10), respectively. Our values are comparable to the values reported previously, which are +0.30±0.06, +0.28±0.02, and -2.46±0.02‰, respectively (Archer et al., 2017; Conway et al., 2013; Moynier et al., 2017). The long-term reproducibility was monitored by repeated measurement of IRMM-3702, which was +0.27±0.05‰ (Figure S4). We also measured the [Zn] and δ^{66}Zn in reference seawater samples, CASS-5, CASS-6, NASS-6, and NASS-7 (Table S3), which were comparable to the reported values (Takano et al., 2017; Yang et al., 2018). Intercomparison exercise was carried out internally in this study. Wen-Hsuan Liao measured the [Zn] and δ^{66}Zn at stations SEATS and TR11, which had been determined previously and independently by Shun-Chung Yang and Shotaro Takano, respectively. The TR11 samples for intercomparison were collected independently by two different laboratories during the KH11-7 cruise. The data agreed well with each other for almost all of the intercomparison samples (Figure 2).

3. Results

3.1. Oceanographic Setting and Hydrographic Parameters

Nine stations from four adjacent oceanic regions were studied, including the SEATS station in the SCS, two stations in the WPS, five stations in the Kuroshio, and one station in the Kuroshio extension area (Figure 1). Four end-member water masses are identified in the T-S diagram of the four studied regions

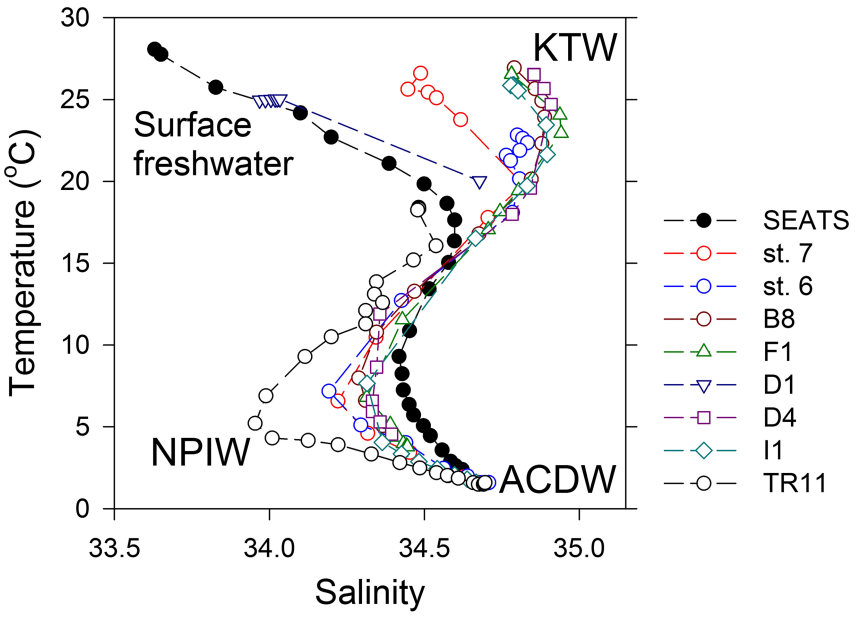

Figure 3. Temperature versus salinity (T-S) diagram of the studied stations. Four major water masses can be identified in the diagram.

(Figure 3), including the Antarctic Circumpolar Deep water, the North Pacific Intermediate water, the Kuroshio Tropical water, and the surface freshwater in the northern SCS. Station TR11 in the Kuroshio extension region possesses a typical T-S feature of the intermediate water of the NWPO. The SEATS station demonstrates a typical feature of the water mass in the northern SCS, high temperature, and low salinity in the surface water and relatively high salinity in the intermediate water. The influence of the northern SCS on the intermediate water is significant for the Kuroshio and WPS stations. The detailed oceanographic settings are described in Text S1 in the supporting information. Major nutrients were determined for all samples collected in this study (Figures S1 and S2). Chlorophyll-*a* concentrations and beam attenuation coefficient were also measured in the surface water for comparison with [Zn] and δ^{66}Zn. The vertical profiles of phosphate and silicate concentrations are presented in Figure S1. Linear relationships between silicate and Zn concentrations are observed for almost all of the stations, except for the SEATS station (Figure S2).

3.2. Spatial Distribution of [Zn] and δ^{66}Zn

All the [Zn] and δ^{66}Zn of all sampling stations are shown in Figure 2. Dissolved [Zn] profiles display a typical nutrient-type distribution with highly varied surface water concentrations ranging from 0.11 to 5.0 nM. The surface [Zn] observed in the Kuroshio extension and the Kuroshio region next to the ECS is significantly lower than the concentrations observed in the SCS and the WPS. Temporally, we observed a significant increase in surface [Zn] in the WPS, from 0.86 to 2.4 nM in summer to 2.0 to 5.0 nM in spring. This may be caused by an additional source of dissolved Zn from aerosol deposition in the surface ocean of the NWPO (Jakuba et al., 2012; Kim et al., 2015). Indeed, aerosol Zn concentrations were 0.11 and 0.81 nmol/m^3 for the summer and spring sampling for the two Taiwanese GEOTRACES cruises, respectively. Similar seasonal variation was also observed from monthly mean aerosol optical depth (AOD) data, a semi-quantitative proxy for aerosol concentrations (Figure S5). For δ^{66}Zn, the surface water of all studied sites exhibited relatively low δ^{66}Zn, ranging from −0.91 to +0.24‰ in the upper 200 m (Figure 2). Some δ^{66}Zn in the euphotic zone possessed relatively light values at station 7 in the WPS and station B8 in the Kuroshio next to the ECS. In the deep water, dissolved [Zn] and δ^{66}Zn increased with depth from the thermocline to 1,000 m. In water deeper than 1,000 m, δ^{66}Zn were relatively constrained, and the values generally ranged from +0.23 to +0.50‰ (Figure 2). δ^{66}Zn showed significant spatial variations in the deep water, with an increasing trend from the SCS and WPS regions to the Kuroshio region to the Kuroshio extension (Figure 2, left to right). The averaged deep water value of all the studied stations, +0.38±0.10‰, was

slightly lower than globally averaged deep water value, +0.47±0.15‰, calculated by published δ^{66}Zn datasets and the data obtained in this study (n = 682).

4. Discussion

4.1. The Deep Water Column of the NPO

We found that dissolved δ^{66}Zn in the deep NWPO is about 0.10 to 0.20‰ lighter than the values reported in the Northeastern Pacific Ocean (Figure 5; Conway & John, 2015). External input of isotopically light Zn is most likely to be the major process causing the spatial variations of δ^{66}Zn in the NPO. The potential processes causing the variations may include particle sinking, sedimentary input, and water mixing.

4.1.1. The impact of aerosol input on the deep water of the SCS and the WPS

In the NWPO, δ^{66}Zn in anthropogenic aerosols (particulate matter 2.5) collected in the SCS (+0.072±0.06‰) was much lower than the averaged δ^{66}Zn in the deep water of the SCS and the WPS (+0.30±0.07‰). Anthropogenic aerosol input may be a possible cause of the spatial variations observed in the deep water of the NPO. Indeed, previous studies have demonstrated that anthropogenic aerosol deposition is the dominant source of most particulate trace metals in the water column of the SCS. The SCS thus serves as an ideal location to investigate the impact of anthropogenic aerosols on marine trace metal cycle due to its high anthropogenic aerosol fluxes (Ho et al., 2007; Ho et al., 2010; Ho et al., 2011). With the available information for physical mixing and particle vertical transport in the SCS, previous studies have established box models to evaluate the relative contribution between physical mixing and sinking particles on trace metal cycling (Ho et al., 2010; Ho et al., 2011; Yang et al., 2012). Here, we have applied a similar approach to evaluate their relative importance on Zn cycling in the three boxes of the water column at the SEATS station (Figure 4). By assuming steady state, Zn residence time with respect to an individual process can be estimated and compared in the three boxes (Figure 4). Due to the relatively high sinking fluxes in the upper water column, Zn residence time in the top two layers with respect to particle sinking is much shorter than the ones estimated from physical mixing (upwelling and horizontal mixing), indicating that the dominant process controlling the Zn cycle in the top two boxes is vertical particle transport. The high particle fluxes in the surface and subsurface water can be attributed to the high aerosol Zn fluxes observed in the region (Figure 4). However, the contribution of particle sinking in deep water is relatively small. The physical transports of water masses laterally and vertically are the primary processes regulating Zn cycling in the deep water (Figure 4).

Residence time estimated by the box model indicates that physical transport is more important than particle sinking for Zn recycling in the deep water of the SCS. The deep water is known to originate from the intermediate water of the WPS at depths ranging from 1,500 to 2,500 m, which inflows from the Luzon Strait to the SCS (Chang et al., 2010; Liu & Gan, 2017). The residence time of the North Pacific Intermediate water was reported as 14–19 years at the zonation of 75 to 1,000 m and 170–230 years from 1,000 to 2,000 m, calculated by using chlorofluorocarbons as tracers (Watanabe et al., 1997). We assume that the residence time of physical mixing at the zonation of 1,000 to 2,000 m of the WPS is also around 200 years. We assume that Zn fluxes of particle sinking in the WPS intermediate water are close to or within the range of one tenth of the values observed in the SCS, which resulted in the fluxes ranging from 0.14 to 1.4 μmol $\cdot m^{-2} \cdot day^{-1}$ in the WPS intermediate water (Figure 4). Then, the estimated Zn residence time of the WPS intermediate water for particle sinking would range from 50 to 500 years. The top-down flux by particle sinking would be one of the major Zn sources in the WPS intermediate water. As the averaged δ^{66}Zn in anthropogenic aerosols collected in the SCS was relatively light, +0.072±0.065‰, δ^{66}Zn in the WPS surface and intermediate water can thus be transformed by anthropogenic aerosol input within the time scales of the residence time. Indeed, we observed significant seasonal variations for [Zn] and δ^{66}Zn in the top 200 m of the WPS, with elevated [Zn] and relatively light δ^{66}Zn during high aerosol deposition season.

Aerosol deposition would also considerably influence the WPS intermediate water, resulting in relatively isotopically light δ^{66}Zn values ranging from 0.21 to 0.39‰ in the water from 500 to 1,500 m (Figure 2). Because WPS intermediate water flows into the SCS and forms the deep water, this may explain the

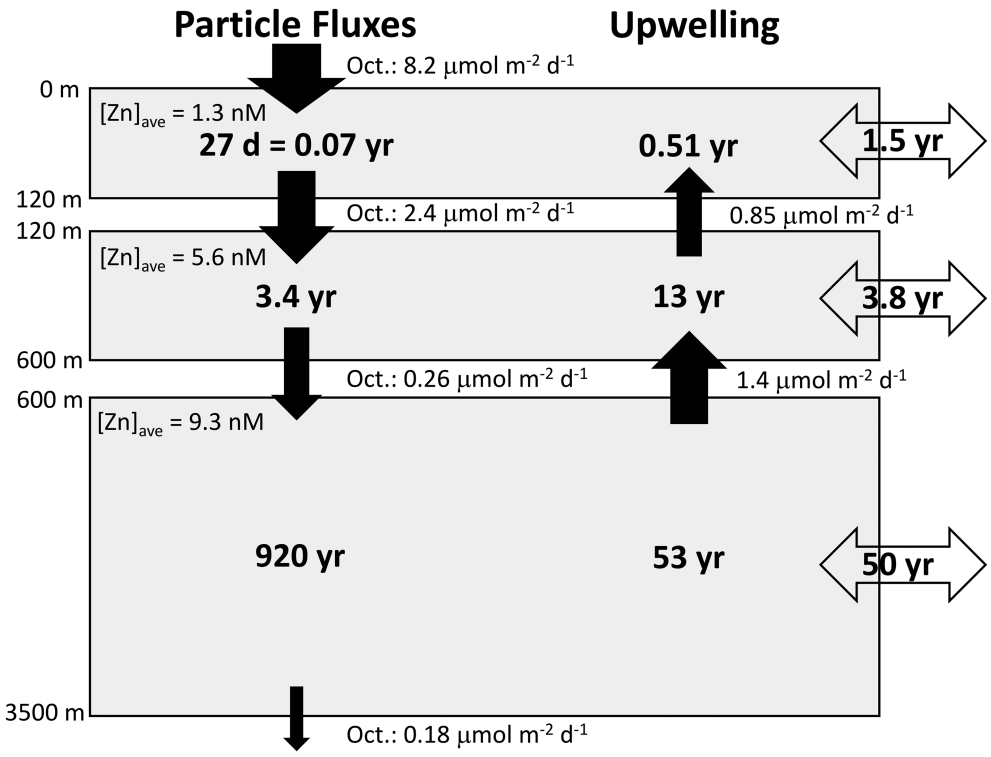

Figure 4. Comparison of residence time estimated by particle sinking and physical transport processes in the water column of the SEATS station. Averaged dissolved Zn concentration was used to calculate total Zn inventory in each box. The fluxes listed next to the sinking particle arrows represent aerosol and sinking fluxes obtained from previous studies in the South China Sea (Ho et al., 2010; Ho et al., 2011). The flux differences between the top and bottom depths of each box represent the decomposed vertical Zn fluxes in the box. Assuming steady state, the residence time can be estimated by dividing the inventory with the flux differences in each box. The upwelling transport fluxes were estimated by using upwelling velocity, 55 m/year (Chen et al., 2001; Ho et al., 2010). The residence time estimated by horizontal transport was 1.5, 3.8, and 50 years in the surface, subsurface, and deep boxes (Yang et al., 2012).

isotopically light δ^{66}Zn values observed in the deep water of the SCS. Based on an inflow flux of 10.2 ±8.8 kg/s reported in Figure 4b of Kaneko et al. (2001), we estimate the residence time of the WPS deep water ranges from 20 to 250 years from 500 m to bottom depth. This indicates a deep water residence time of around 250 years. Other studies have reported the circulation ^{14}C age of CDW in the Pacific Ocean as 295 years (Matsumoto, 2007). By using different water mass entry and exit region pairs in the Pacific Ocean, a steady state offline ocean circulation model estimated the residence time of the deep water in the Northern Pacific Ocean to range from 177 to 415 years (Primeau & Holzer, 2006). Assuming that particle sinking fluxes in the WPS deep water are comparable to the values observed in the SCS, the residence time estimated by particle sinking would be within the same order of magnitude of the residence time of physical transport for Zn recycling in the WPS deep water. Therefore, the input of anthropogenic aerosols may be a potential source of the slightly light dissolved Zn in the deep water of the WPS.

4.1.2. Other potential causes of deep water spatial δ^{66}Zn variations

In addition to aerosol deposition, sedimentary Zn input has also been proposed as a possible source to the intermediate water of the subarctic NPO by using Zn* as an indicator (Kim et al., 2017). Benthic nepheloid layers may be another potential external trace metal source and may exist in the deep water at the west end of the NPO (Gardner et al., 2018). To estimate extra Zn input in the water column, Zn* is used to quantitatively express the external Zn input, which is calculated by silicate concentrations and its linear relationship with [Zn]. We have observed positive Zn* values in the deep water of the SEATS station and stations 6 and 7 in the WPS, implying a potential Zn input in the regions (Figure S3). Similar spatial variations of Zn* and δ^{66}Zn were observed in the deep water of the North Atlantic Ocean (NAO). Conway and John (2014,

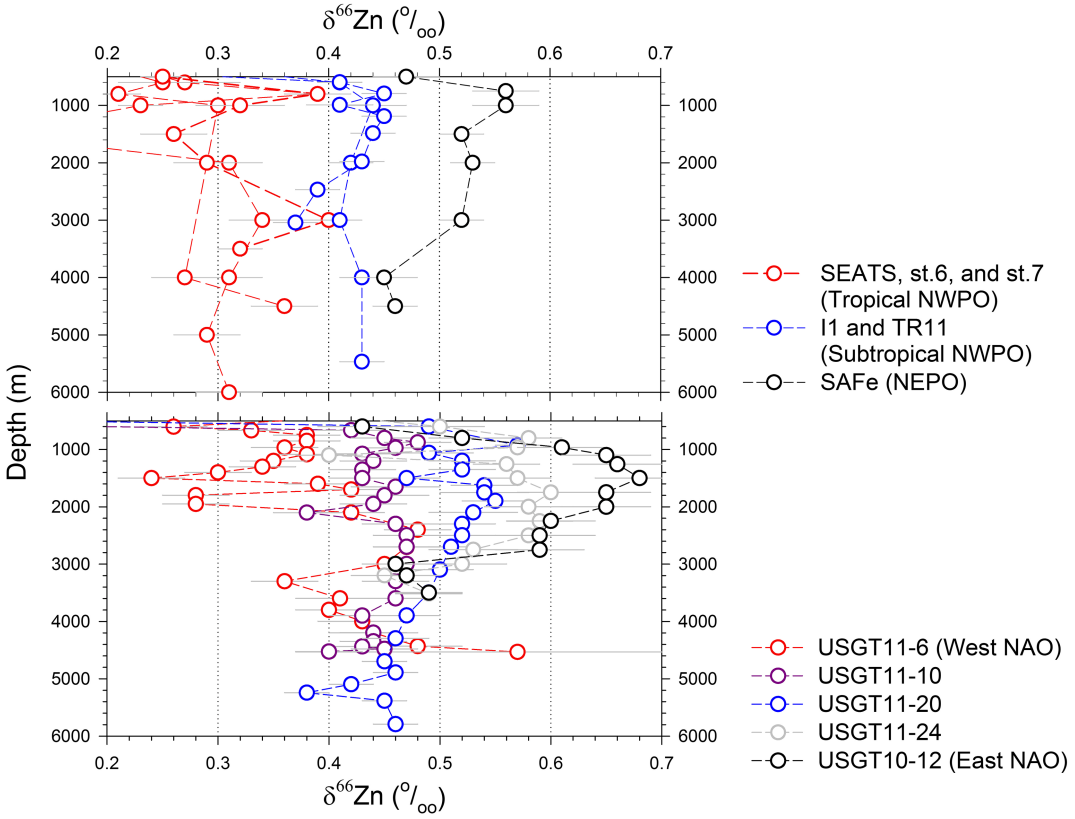

Figure 5. The spatial variations of δ^{66}Zn in the water column of the studied sites in the Northwestern Pacific Ocean (NWPO), the SAFe station (Conway & John, 2015), and the North Atlantic Ocean (NAO; Conway & John, 2014).

2015) found high Zn* values with isotopically light δ^{66}Zn in the deep water of the NAO and also proposed that the input of dissolved benthic Zn might be the major cause of the spatial variations. Assuming that the benthic input is the major source of the light Zn in the NWPO, the δ^{66}Zn value of benthic Zn input can be estimated by an isotope mass balance approach in the NWPO. Using station 6 and TR11 as the west and east boundary stations and attributing the concentration and δ^{66}Zn differences (9.7 versus 8.6 nM and 0.36 and 0.43‰) between the two stations to benthic input, we estimated the δ^{66}Zn value of benthic input to be −0.19‰. This calculated benthic δ^{66}Zn value is comparable to the values calculated for margin sediment input in the NAO (Conway & John, 2014) and the authigenic Zn from Pacific margin sediments (Little et al., 2016). The results of these two studies were also based on isotope mass balance calculation. As δ^{66}Zn field measurements of benthic input are not available, further studies are needed to validate this δ^{66}Zn value.

With a known δ^{66}Zn signature from benthic input, we may use a box model to evaluate the possibility that the isotopically light input may cause the spatial variations. Westerlund et al. (1986) reported that the benthic dissolved Zn flux is 1.9 $\mu mol \cdot m^{-2} \cdot day^{-1}$ in a shallow water coastal environment. However, no systematic study has been carried out for the benthic input of Zn in the open ocean to date. The elemental and isotopic compositions are assumed to vary from +0.45‰ and 9 nM to +0.30‰ and 10 nM in the deep water box from 600 to 3,500 m (Figure S6). Simply assuming that benthic Zn flux ranges from 1 to 0.1 $\mu mol \cdot m^{-2} \cdot day^{-1}$ and the δ^{66}Zn signature of benthic input as −0.19‰, the estimated turnover time by benthic input would be 42 to 420 years in the deep water. Sedimentary input may thus be an excess Zn source in the deep water, in addition to the desorption of scavenged Zn and Zn transported from the SO (Roshan et al., 2018; Weber et al., 2018). In addition, although hydrothermal input can be an important trace metal source in the deep water of the Pacific Ocean (Resing et al., 2015; John et al., 2017), it remains unknown that hydrothermal input is a major Zn source in the deep water of the NWPO or not. To better constrain the potential

importance of the deep water sources, more transect studies from coastal regions to the open ocean are needed to better quantify the relative contribution of the inputs in a global scale.

4.2. The Upper Water Column

4.2.1. Distribution Pattern of [Zn] and δ^{66}Zn in the NWPO and Other Oceanic Regions

Globally comprehensive studies on dissolved Cd isotope composition have provided us insight on how physical and biogeochemical processes regulate the isotope composition of Zn in the marine water column. Cd isotope composition in the surface water is mainly regulated by phytoplankton uptake and exhibits a relatively high value in dissolved pool and relatively low value in biogenic particles (Abouchami et al., 2011; Abouchami et al., 2014; Ripperger et al., 2007; Yang et al., 2012; Yang et al., 2015). Early studies suggested that the Cd fractionation pattern observed mostly follows a typical closed Rayleigh fractionation system in the marine water column (Abouchami et al., 2011; Ripperger et al., 2007). However, later studies showed that a closed-system model cannot explain the fractionation pattern for sample concentrations less than 0.1 nM (Gault-Ringold et al., 2012; Xie et al., 2017). Xie et al. (2017) proposed a steady-state open system to further explain the Cd fractionation pattern. Yang et al. (2018) also showed that Cd isotope fractionation can match either a closed or open system model, depending on the relative contribution of physical and biogeochemical processes on its cycling. Overall, Cd fractionation patterns shown by either closed or open system models exhibit fractionation factors greater than 1, indicating that particulate phase is enriched with relatively light Cd due to biological uptake.

Although Zn is a biologically essential trace metal, dissolved δ^{66}Zn mostly exhibits an isotopically light signature in the surface ocean (Conway & John, 2014, 2015), in contrast to the distribution pattern of Cd isotope composition. However, some studies reported that dissolved δ^{66}Zn may exhibit insignificant fractionation or even isotopically heavy signature in oceanic surface water, including the studies observed in the SO, the Tasman Sea, the SEPO, and the subarctic Northeastern Pacific Ocean (Samanta et al., 2017; Sieber et al., 2019; Vance et al., 2019; Wang et al., 2019; Zhao et al., 2014). Since culture studies showed that adsorbed Zn is isotopically heavy relative to intracellular Zn, scavenging has first been proposed to be the major process causing the relatively light Zn feature in the surface water (John et al., 2007; John & Conway, 2014). A recent study using model calculation approach suggested that physical mixing may be one of the processes causing δ^{66}Zn variation in the surface water of the Northeastern Pacific Ocean, which may be up to 0.3‰ (Vance et al., 2019). In addition, Liao and Ho (2018) found that particulate Zn concentrations are significantly correlated with aerosol Zn fluxes in the global ocean, implying the importance of aerosol deposition on Zn cycling in the surface ocean. In brief, the processes proposed for causing the fractionation in the surface water include biological uptake, scavenging, mixing, and external inputs. The relative contribution of the various processes on Zn fractionation remains largely unclear among different oceanic regions.

To investigate the direction of Zn fractionation, we may apply closed or open system fractionation models to show the relationship between [Zn] and δ^{66}Zn and to evaluate the importance of scavenging process in the surface water. If Zn fits in the closed system model, its isotopic ratios would possess a linear relationship with its concentrations in log scale. In the open system model, it is assumed that the supply of Zn from subsurface water balances the vertical export of sinking particles. Thus, if Zn fits in the open system model, its isotopic ratios would approach a constant value with decreasing concentrations. The equations of the closed and open system models are listed below, respectively, where fractionation factor (α) is equal to $R_{\text{seawater}}/R_{\text{particle}}$ and the R in the factor is defined as ^{66}Zn/^{64}Zn.

$$\delta^{66}\text{Zn}_{\text{surf}} = \delta^{66}\text{Zn}_{\text{initial}} - 10^3 \cdot (1 - 1/\alpha) \cdot \ln\left([\text{Zn}]_{\text{surf}}/[\text{Zn}]_{\text{initial}}\right) \quad (3)$$

$$\delta^{66}\text{Zn}_{\text{surf}} = \delta^{66}\text{Zn}_{\text{initial}} + 10^3 \cdot (1 - 1/\alpha) \cdot \left(1 - [\text{Zn}]_{\text{surf}}/[\text{Zn}]_{\text{initial}}\right) \quad (4)$$

We used δ^{66}Zn versus [Zn] plots to demonstrate the data distribution pattern in the upper 1,000 m of the water columns. For our study, we have separated the data obtained based on the hydrographic distinction of the stations (Figure 1) into the SCS, the WPS, the Kuroshio adjacent to the ECS, and the Kuroshio extension region (KuroEx). The distribution pattern between δ^{66}Zn and [Zn] shows that dissolved δ^{66}Zn decrease with decreasing [Zn] for all regions so that the fractionation factors are all less than 1 in both models (Figure 6a). This pattern indicates that the dissolved phase is lighter than the particulate phase, in

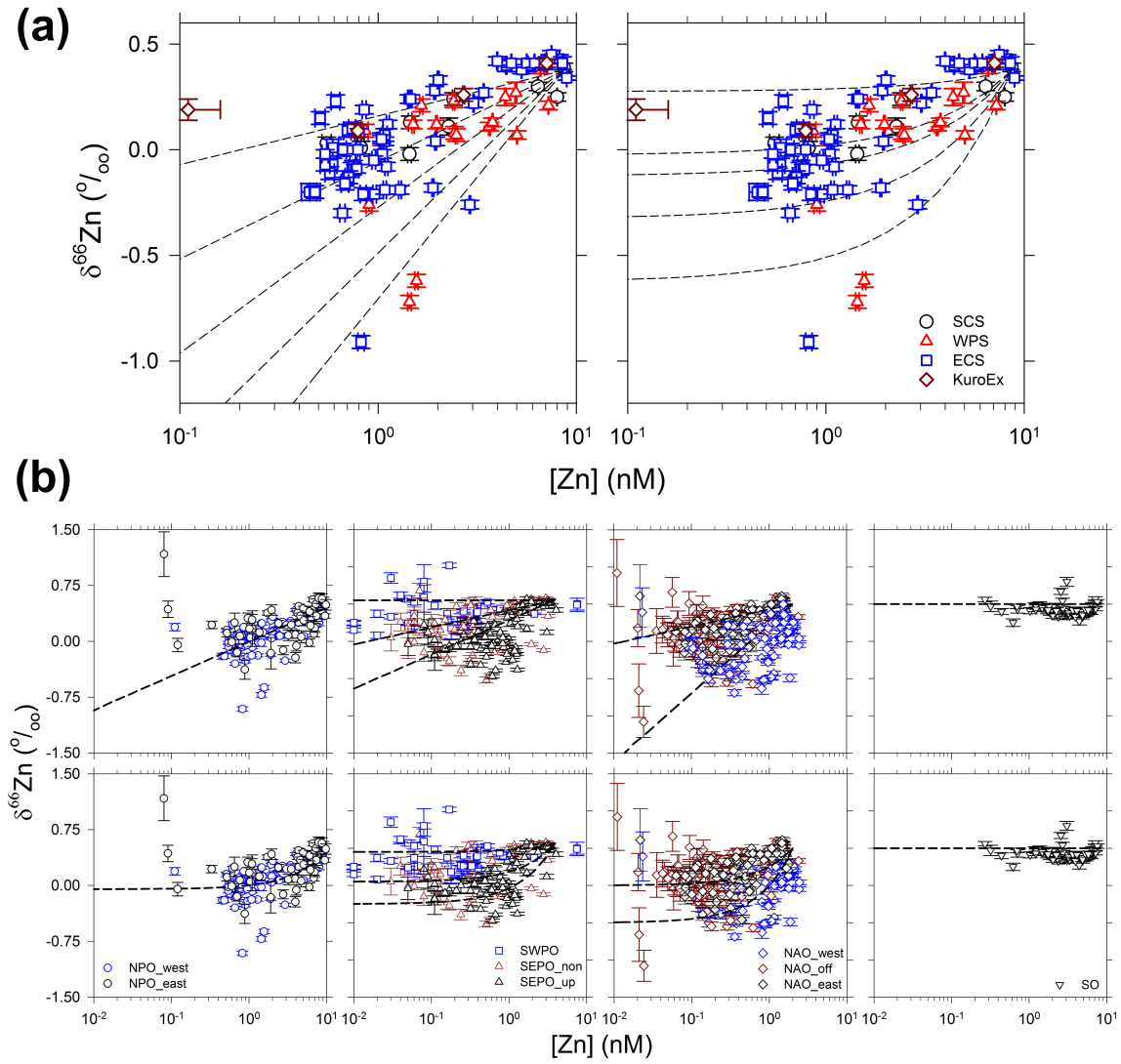

Figure 6. The comparison of Zn fractionation patterns in the upper 1000 m water column of the global ocean fitted by closed and open system models. Upper panel (a) shows data obtained in the Northwestern Pacific Ocean (NWPO) and its marginal seas. The fractionation lines of Zn systematics for both closed (left) and open system (right) steady-state models were calculated with δ^{66}Zn and [Zn] initial values at 0.38‰ and 8.7 nM, respectively. The initial values are the averaged values of 1,000 m at all the stations in this study. Lower panel (b) shows the data compiled from different oceanic regions globally. Data for the west end of the North Pacific Ocean (NPO) were obtained in this study; data for the east end are from John and Conway (2014), Conway and John (2015), and Vance et al. (2019). Data for the SWPO are from Samanta et al. (2017), and the Southeastern Pacific Ocean (SEPO) data are from John et al. (2017). Data for the North Atlantic Ocean (NAO) are from Conway and John (2014). Data for the SO are from Zhao et al. (2014) and Wang et al. (2019). We used both closed (top row) and open system (bottom row) models to demonstrate the fractionation pattern in the global ocean. The initial δ^{66}Zn and [Zn] averaged values at 1,000 m are 0.45, 0.55, 0.5, and 0.5‰ and 9.8, 3.8, 2, and 8.4 nM for the NPO, the South Pacific Ocean (SPO), the NAO, and the Southern Ocean (SO), respectively.

contrast to the situation with Cd. We thus further compiled all of the published δ^{66}Zn and [Zn] data to evaluate the role of scavenging in the surface water globally. The distribution pattern of the δ^{66}Zn and [Zn] data obtained in the NAO and the SEPO is comparable to the one observed in our study (Figure 6b). Since scavenging may preferentially remove isotopically heavy Zn from dissolved pool, scavenging can be one of the major mechanisms removing isotopically heavy Zn in the surface water (John et al., 2007; John & Conway, 2014). However, the data distribution is relatively scattered and not constrained to any specific fractionation factors (Figure 6b), suggesting that multiple processes are involved in regulating Zn fractionation in the surface water. In addition to internal processes, such as biological uptake or scavenging, external processes are potential important factors on regulating the fractionation, which may at least include mixing and external input.

4.2.2. Processes Determining [Zn] and δ^{66}Zn in the Surface Ocean

In terms of biological uptake, culture experiments have demonstrated that some phytoplankton species take up isotopically light Zn relative to the bulk medium (John et al., 2007; John & Conway, 2014; Köbberich & Vance, 2017; Köbberich & Vance, 2019; Samanta et al., 2018), with an isotopic difference approximately +0.2 to +0.4‰. In terms of field study, Samanta et al. (2017) observed isotopically heavy dissolved Zn in a high biomass season in the upper water of the Southwestern Pacific Ocean (SWPO), where aerosol deposition is extremely low, supporting that phytoplankton may preferentially take up isotopically light Zn. The other field study in subarctic Northeastern Pacific Ocean also found isotopically heavy values in the top 50 m where chlorophyll-*a* concentrations were highest, with an isotopically light value right below the surface water. The sequentially contrasting fractionation pattern was attributed to biological uptake and shallow remineralization in the surface water (Vance et al., 2019). On the other hand, a recent study observed an isotopic difference between organic ligand chelated Zn (e.g., EDTA) and inorganic Zn (Marković et al., 2017). Thus, it has been proposed that the uptake of light Zn observed in culture experiments can be mainly attributed to ligand complexation effect so that Zn fractionation of biological uptake may be insignificant (Köbberich & Vance, 2019; Vance et al., 2019; Wang et al., 2019). However, it should also be noted that phytoplankton would overexpress nonspecific divalent metal transporter under Fe limiting condition (Lane et al., 2008; Lane et al., 2009) and enhance the uptake of other divalent trace metals. Assuming that the transporters possess high affinity for Zn uptake, this would then result in insignificant Zn fractionation in the surface water of the SO. Here, we propose that the insignificant fractionation in the SO may be attributed to the elevated uptake of Zn by nonspecific divalent metal transporter, which occurs under Fe limiting condition.

Dissolved δ^{66}Zn observed in most of the oceanic regions studied, including the NAO and the SEPO, is generally isotopically light. Dissolved δ^{66}Zn observed in this study also possess isotopically light signature in the surface water (Figures 2 and 6a). In addition to the seminal culture study (John et al., 2007), a recent culture study also indicated that Zn adsorption onto the surface-bound Fe-hydroxides may cause bulk δ^{66}Zn to be isotopically heavy (Köbberich & Vance, 2018). Scavenging seems to be a major process causing the surface isotopically light Zn signature in the oceans. Although a recent simulation study suggested that scavenging would play a role on regulating Zn distribution globally, this simulation study argued that scavenging Zn may only account for a small portion of total Zn mass, ~0.5% in the surface water and <0.01% in the deep water (Weber et al., 2018). In addition, a large-scale transect study in the Atlantic Ocean indicated that the effect of scavenging is insignificant for the distribution of dissolved Zn (Middag et al., 2019). The role of scavenging on Zn and δ^{66}Zn distribution seems to be inconsistent among different oceanic regions.

On the other hand, recent studies found that physical mixing is a dominant process regulating Zn elemental and isotopic distribution and variations spatially (Middag et al., 2019; Vance et al., 2019). Middag et al. (2019) found that dissolved [Zn] distribution in the Atlantic Ocean is dominated by advection and mixing rather than regional remineralization and scavenging. Vance et al. (2019) used a simple 1-D model to evaluate the impact of mixing and suggested that mixing may cause the isotopic variations up to 0.3‰ in the surface water. These evidences support that physical mixing is an important factor on causing δ^{66}Zn variation in marine water column globally, particularly in the deep water where δ^{66}Zn are relatively constrained. For the NWPO, the relatively constrained deep water δ^{66}Zn values indicate that physical mixing is the dominant process determining δ^{66}Zn variation in the deep water. However, in the surface and subsurface water of the SCS, our box model results show that physical mixing plays a minor role on Zn cycling (Figure 4). In brief, physical mixing plays a dominant role on regulating [Zn] and δ^{66}Zn in the deep water, but its role on regulating Zn cycling in the surface water seems to be spatially specific.

Several lines of evidence show that external input may be a critical factor determining δ^{66}Zn in the surface water of some oceanic regions. Some relatively high δ^{66}Zn values were observed at the top depths at some NAO stations (Conway & John, 2014). Similarly, we also observed relatively high δ^{66}Zn at the very surface depths in the top 200 m of stations 7, B8, F1, and D4 in this study. Previous studies also observed elevated dissolved [Zn] in the surface water of the high-latitude NWPO regions (Jakuba et al., 2012; Kim et al., 2015). All of these observations indicate that aerosol deposition is a major external source of Zn in the surface waters. It should be noted that anthropogenic aerosol Zn is a dominant portion in bulk aerosol Zn. Even in the oceanic regions near the Saharan desert, anthropogenic aerosol Zn accounted for more than 55% of total aerosol Zn (Dong et al., 2013). Zn solubility in bulk aerosols is thus generally high in almost all of

the open oceanic regions studied, usually higher than 70% (e.g., Chance et al., 2015; Shelley et al., 2018). In terms of aerosol δ^{66}Zn, a recent study compiled published datasets and showed that anthropogenic aerosol Zn is isotopically lighter than lithogenic materials with δ^{66}Zn to be around +0.3‰ (Rosca et al., 2018). The averaged δ^{66}Zn in anthropogenic aerosols collected in the SCS was +0.072±0.065‰, also lighter than lithogenic dusts. Anthropogenic aerosol Zn input may thus be an important source causing dissolved δ^{66}Zn to become isotopically light in most of the surface water of the NWPO.

Since δ^{66}Zn values are generally isotopically light in the surface water of the NWPO, the fractionation effects of biological uptake and ligand chelation are supposed to be relatively insignificant. Similarly, subsurface water mixing is unlikely to be a major source of the isotopically light δ^{66}Zn in the NWPO surface water. Based on the discussion mentioned above, anthropogenic aerosol deposition is thus most likely to be the dominant cause of the light signature in the surface water of the NWPO. Indeed, the dissolved δ^{66}Zn in the top 200 m of the WPS were comparable to aerosol δ^{66}Zn in a high aerosol deposition period (blue symbol in Figure 2), supporting that external aerosol input can be the dominant Zn source in the surface water. We thus propose that aerosol deposition is an important external Zn source causing [Zn] and δ^{66}Zn variations in the surface water, particularly in the surface water receiving high aerosol deposition, such as the NWPO.

4.2.3. Comparison of [Zn] and δ^{66}Zn in the Surface Water

To examine the distribution patterns of [Zn] and δ^{66}Zn among different oceanic regions and their association patterns with aerosol deposition, we compiled all published δ^{66}Zn and [Zn] values in the upper 200 m among different oceanic regions (Figure 7). We have first separated the data based on their locations, the Southern Pacific Ocean (SPO), the NAO, and the NPO. In the SPO, we have separated the data into the SWPO and the nonupwelling and upwelling regions of SEPO (Figure 7a). For the NAO, we have separated the data into three regions based on the distribution of AOD, including the high AOD stations in the eastern NAO (high-east), the low AOD stations in middle NAO (low-mid), and high AOD stations in the western NAO (high-west; Figures 7b and 7d). It should be noted that AOD is a useful indicator for aerosol concentrations but not quantitatively equivalent to the deposition flux (Mahowald et al., 2009).

In terms of the distribution range of [Zn], we found that [Zn] in the NPO are statistically higher than the values observed in the SPO and the NAO ($p<0.05$; Figure 7). For the SPO, the [Zn] observed in the upwelling region of the SEPO (circle points) are higher than the ones observed in the nonupwelling region of the SEPO and the SWPO (triangle points; $p<0.05$; Figure 7a). Similarly, for the NAO, the high-west stations where anthropogenic aerosol deposition is relatively high, [Zn] are higher than the ones in the low-mid stations where aerosol deposition is relatively low (Figure 7d). At the NAO high-east stations, where lithogenic dust deposition is extremely high, [Zn] are relatively low but higher than the low-mid stations. The variations of dissolved [Zn] are significantly and positively correlated to AOD among different oceanic regions (Figure 7e).

In terms of δ^{66}Zn, the values in the upwelling region of the SEPO are isotopically lighter than the nonupwelling region and the SWPO. We propose that high particle concentrations and dissolved Zn input may enhance scavenging effect and cause isotopically light dissolved δ^{66}Zn values (Figure 7a). For the NAO, the δ^{66}Zn were relatively light at the NAO high-west stations where anthropogenic aerosol Zn deposition were relatively high; contrarily, δ^{66}Zn were relatively heavy at the NAO low-mid stations where aerosol deposition was relatively low (Figure 7d). However, δ^{66}Zn are relatively heavy at the NAO high-east stations where lithogenic dust deposition was extremely high. Isotopically heavy insoluble lithogenic Zn may be the major cause for the relatively heavy δ^{66}Zn observed at the high-east stations. For the NAO high-west stations, in addition to the direct effect of light anthropogenic aerosol Zn input, scavenging might further fractionate Zn to result in even lighter δ^{66}Zn values in the surface water.

Our previous study demonstrated that particulate Zn concentrations in the surface water are significantly correlated with aerosol Zn fluxes in the oceanic regions studied globally, implying the importance of aerosol deposition on Zn cycling in the surface ocean (Liao & Ho, 2018). Particularly, anthropogenic aerosol flux in the NWPO is the highest among the oceanic regions. Anthropogenic aerosols generated from East Asia are transported to the subarctic NPO by the seasonal monsoon and the Westerlies, witnessed by the relatively high annual average AOD (Figure 7d). Indeed, more than 90% of available [Zn] data in the surface water compiled in the NPO are greater than 0.5 nM, possessing the highest averaged [Zn] among the major

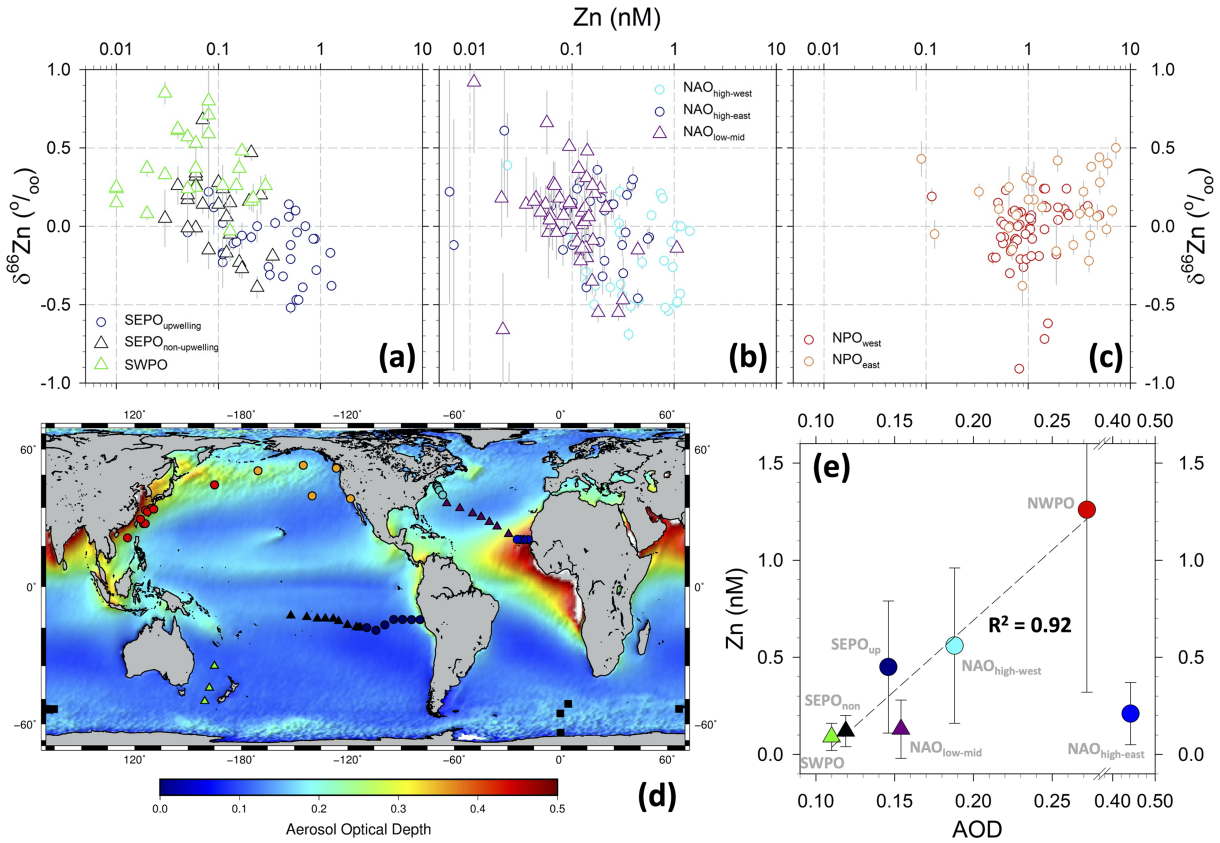

Figure 7. The distribution patterns of [Zn] and δ^{66}Zn in the upper 200 m of (a) the South Pacific Ocean (SPO), (b) the North Atlantic Ocean (NAO), and (c) the North Pacific Ocean (NPO). (d) Sampling locations of the data and annual average aerosol optical depth (AOD) in the global ocean. (e) The correlation between AOD and average [Zn] in the top 200 m among the different oceanic regions (e). The error bars of the average [Zn] stand for one standard deviation of all data obtained from individual oceanic region. We have separated the sampling stations among different oceanic regions to high and low aerosol deposition regions based on AOD values. The low external input regions include the nonupwelling Southeastern Pacific Ocean (SEPO) and the open ocean stations in the NAO, which are shown with triangle symbols. The high external input regions and high upwelling stations are shown with circle symbols. The criteria of upwelling and nonupwelling stations were mentioned in Ohnemus et al. (2017). AOD data are obtained by averaging annual values from 2001 to 2017 (Moderate Resolution Imaging Spectroradiometer [MODIS]/Aqua, Near-Earth Object [NEO], National Aeronautics and Space Administration [NASA]).

oceans (Figures 7c and 7e). We also calculated Zn* for the data obtained in the upper 1,000 m of the NWPO. Most of the Zn* values are positive, suggesting external Zn input in the surface ocean, highly likely to be aerosol deposition (Figure S7). The δ^{66}Zn observed in the NPO also showed an isotopically light signature similar to the high-west stations of the NAO where anthropogenic aerosols are likely to be the dominant Zn source in bulk aerosols. In brief, the comparison of the global datasets indicates that external soluble Zn input in the surface water is closely associated with elevated [Zn] and lighter δ^{66}Zn value. Aerosol deposition is most likely to be the major cause for the variations of surface water [Zn] and δ^{66}Zn in oceanic regions with high AOD (Figure 7).

5. Conclusion

We have observed relatively light dissolved δ^{66}Zn and significant spatial variations in the deep ocean of the NWPO and its marginal seas. The box model calculation indicates that the spatial variations in the NWPO deep water are caused by the external supply of isotopically light Zn, most likely from anthropogenic aerosol deposition or sedimentary input. To explain the δ^{66}Zn variations in the surface water, we hypothesize that external Zn addition, such as aerosol deposition, is a major cause to change δ^{66}Zn values in addition to the internal processes of biological uptake and scavenging. This argument is supported by the consistent distribution patterns of [Zn] and δ^{66}Zn obtained from different oceanic regions with highly varied AOD. Anthropogenic aerosol deposition may thus be a critical process to cause [Zn] and δ^{66}Zn variations in the

surface water. Future studies on oceanic regions with contrasting aerosol deposition spatially or seasonally would validate the importance of aerosol deposition on Zn cycling in the surface water.

Acknowledgments
AcknowledgementWe thank two anonymous reviewers, Zanna Chase, and handling editors for their invaluable comments, which have significantly improved the quality of our manuscript. We thank Der-Chuen Lee, Bo-Shian Wang, Chih-Ping Lee, Tsai-Luen Yu, Claudia Chern, Vineet Goswami, Jing Zhang, and the personnel of TORI (Taiwan Ocean Research Institute), R/V Ocean Research I, Ocean Research V, and Hakuho-maru for their technical assistance. We thank Phoebe Lam, George T. F. Wong, and Ching-Ling Wei for providing helpful comments on this manuscript. This study was financially supported by Taiwan Ministry of Science and Technology grants 105-2119-M-001-039-MY3 and 108-2611-M-001-006-MY3, the Career Development Award of Tung-Yuan Ho from Academia Sinica, and partially by Japan GEOTRACES program and the International Joint Usage/Research Project with ICR, Kyoto University. The raw data are archived at PANGAEA (https://doi.pangaea.de/10.1594/PANGAEA.909738).

References

Abouchami, W., Galer, S. J. G., de Baar, H. J. W., Alderkamp, A. C., Middag, R., Laan, P., et al. (2011). Modulation of the Southern Ocean cadmium isotope signature by ocean circulation and primary productivity. *Earth and Planetary Science Letters*, *305*(1-2), 83–91. https://doi.org/10.1016/j.epsl.2011.02.044

Abouchami, W., Galer, S. J. G., de Baar, H. J. W., Middag, R., Vance, D., Zhao, Y., et al. (2014). Biogeochemical cycling of cadmium isotopes in the Southern Ocean along the Zero Meridian. *Geochimica et Cosmochimica Acta*, *127*(Supplement C), 348–367. https://doi.org/10.1016/j.gca.2013.10.022

Anderson, R., & Henderson, G. (2005). PROGRAM UPDATE|GEOTRACES—A global study of the marine biogeochemical cycles of trace elements and their isotopes. *Oceanography*, *18*(3), 76–79. https://doi.org/10.5670/oceanog.2005.31

Archer, C., Andersen, M. B., Cloquet, C., Conway, T. M., Dong, S., Ellwood, M., et al. (2017). Inter-calibration of a proposed new primary reference standard AA-ETH Zn for zinc isotopic analysis. *Journal of Analytical Atomic Spectrometry*, *32*(2), 415–419. https://doi.org/10.1039/c6ja00282j

Bermin, J., Vance, D., Archer, C., & Statham, P. J. (2006). The determination of the isotopic composition of Cu and Zn in seawater. *Chemical Geology*, *226*(3), 280–297. https://doi.org/10.1016/j.chemgeo.2005.09.025

Bruland, K. W. (1980). Oceanographic distributions of cadmium, zinc, nickel, and copper in the North Pacific. *Earth and Planetary Science Letters*, *47*(2), 176–198. https://doi.org/10.1016/0012-821X(80)90035-7

Bruland, K. W., Knauer, G. A., & Martin, J. H. (1978). Zinc in north-east Pacific water. *Nature*, *271*(5647), 741–743. https://doi.org/10.1038/271741a0

Chance, R., Jickells, T. D., & Baker, A. R. (2015). Atmospheric trace metal concentrations, solubility and deposition fluxes in remote marine air over the south-east Atlantic. *Marine Chemistry*, *177*, 45–56. https://doi.org/10.1016/j.marchem.2015.06.028

Chang, Y.-T., Hsu, W.-L., Tai, J.-H., Tang, T. Y., Chang, M.-H., & Chao, S.-Y. (2010). Cold deep water in the South China Sea. *Journal of Oceanography*, *66*(2), 183–190. https://doi.org/10.1007/s10872-010-0016-x

Chen, C.-T. A., Wang, S.-L., Wang, B.-J., & Pai, S.-C. (2001). Nutrient budgets for the South China Sea basin. *Marine Chemistry*, *75*(4), 281–300. https://doi.org/10.1016/s0304-4203(01)00041-x

Chen, S., Liu, Y., Hu, J., Zhang, Z., Hou, Z., Huang, F., & Yu, H. (2016). Zinc isotopic compositions of NIST SRM 683 and whole-rock reference materials. *Geostandards and Geoanalytical Research*, *40*(3), 417–432. https://doi.org/10.1111/j.1751-908X.2015.00377.x

Chester, R., & Jickells, T. (2012). The transport of material to the oceans: The atmospheric pathway. In *Marine Geochemistry* (pp. 52–82). Chichester, UK: John Wiley & Sons, Ltd.

Conway, T. M., & John, S. G. (2014). The biogeochemical cycling of zinc and zinc isotopes in the North Atlantic Ocean. *Global Biogeochemical Cycles*, *28*, 1111–1128. https://doi.org/10.1002/2014GB004862

Conway, T. M., & John, S. G. (2015). The cycling of iron, zinc and cadmium in the North East Pacific Ocean—Insights from stable isotopes. *Geochimica et Cosmochimica Acta*, *164*, 262–283. https://doi.org/10.1016/j.gca.2015.05.023

Conway, T. M., Rosenberg, A. D., Adkins, J. F., & John, S. G. (2013). A new method for precise determination of iron, zinc and cadmium stable isotope ratios in seawater by double-spike mass spectrometry. *Analytica Chimica Acta*, *793*, 44–52. https://doi.org/10.1016/j.aca.2013.07.025

Coutaud, A., Meheut, M., Viers, J., Rols, J.-L., & Pokrovsky, O. S. (2014). Zn isotope fractionation during interaction with phototrophic biofilm. *Chemical Geology*, *390*, 46–60. https://doi.org/10.1016/j.chemgeo.2014.10.004

de Souza, G. F., Khatiwala, S. P., Hain, M. P., Little, S. H., & Vance, D. (2018). On the origin of the marine zinc–silicon correlation. *Earth and Planetary Science Letters*, *492*, 22–34. https://doi.org/10.1016/j.epsl.2018.03.050

Dong, S., Weiss, D. J., Strekopytov, S., Kreissig, K., Sun, Y., Baker, A. R., & Formenti, P. (2013). Stable isotope ratio measurements of Cu and Zn in mineral dust (bulk and size fractions) from the Taklimakan Desert and the Sahel and in aerosols from the eastern tropical North Atlantic Ocean. *Talanta*, *114*, 103–109. https://doi.org/10.1016/j.talanta.2013.03.062

Gardner, W. D., Jo Richardson, M., Mishonov, A. V., & Biscaye, P. E. (2018). Global comparison of benthic nepheloid layers based on 52 years of nephelometer and transmissometer measurements. *Progress in Oceanography*, *168*, 100–111. https://doi.org/10.1016/j.pocean.2018.09.008

Gault-Ringold, M., Adu, T., Stirling, C. H., Frew, R. D., & Hunter, K. A. (2012). Anomalous biogeochemical behavior of cadmium in subantarctic surface waters: Mechanistic constraints from cadmium isotopes. *Earth and Planetary Science Letters*, *341-344*, 94–103. https://doi.org/10.1016/j.epsl.2012.06.005

Ho, T.-Y., Chou, W.-C., Lin, H.-L., & Sheu, D. D. (2011). Trace metal cycling in the deep water of the South China Sea: The composition, sources, and fluxes of sinking particles. *Limnology and Oceanography*, *56*(4), 1225–1243. https://doi.org/10.4319/lo.2011.56.4.1225

Ho, T.-Y., Chou, W.-C., Wei, C.-L., Lin, F.-J., Wong, G. T. F., & Lin, H.-L. (2010). Trace metal cycling in the surface water of the South China Sea: Vertical fluxes, composition, and sources. *Limnology and Oceanography*, *55*(5), 1807–1820. https://doi.org/10.4319/lo.2010.55.5.1807

Ho, T.-Y., Wen, L.-S., You, C.-F., & Lee, D.-C. (2007). The trace metal composition of size-fractionated plankton in the South China Sea: Biotic versus abiotic sources. *Limnology and Oceanography*, *52*(5), 1776–1788. https://doi.org/10.4319/lo.2007.52.5.1776

Jakuba, R. W., Saito, M. A., Moffett, J. W., & Xu, Y. (2012). Dissolved zinc in the subarctic North Pacific and Bering Sea: Its distribution, speciation, and importance to primary producers. *Global Biogeochemical Cycles*, *26*, GB2015. https://doi.org/10.1029/2010gb004004

Janssen, D. J., & Cullen, J. T. (2015). Decoupling of zinc and silicic acid in the subarctic northeast Pacific interior. *Marine Chemistry*, *177*, 124–133. https://doi.org/10.1016/j.marchem.2015.03.014

John, S. G. (2012). Optimizing sample and spike concentrations for isotopic analysis by double-spike ICPMS. *Journal of Analytical Atomic Spectrometry*, *27*(12). https://doi.org/10.1039/c2ja30215b

John, S. G., & Conway, T. M. (2014). A role for scavenging in the marine biogeochemical cycling of zinc and zinc isotopes. *Earth and Planetary Science Letters*, *394*(Supplement C), 159–167. https://doi.org/10.1016/j.epsl.2014.02.053

John, S. G., Geis, R. W., Saito, M. A., & Boyle, E. A. (2007). Zinc isotope fractionation during high-affinity and low-affinity zinc transport by the marine diatomThalassiosira oceanica. *Limnology and Oceanography*, *52*(6), 2710–2714. https://doi.org/10.4319/lo.2007.52.6.2710

John, S. G., Helgoe, J., & Townsend, E. (2017). Biogeochemical cycling of Zn and Cd and their stable isotopes in the Eastern Tropical South Pacific. *Marine Chemistry*, *201*, 256–262. https://doi.org/10.1016/j.marchem.2017.06.001

Kaneko, I., Takatsuki, Y., & Kamiya, H. (2001). Circulation of intermediate and deep waters in the Philippine Sea. *Journal of Oceanography*, *57*(4), 397–420. https://doi.org/10.1023/a:1021565031846

Kim, T., Obata, H., Kondo, Y., Ogawa, H., & Gamo, T. (2015). Distribution and speciation of dissolved zinc in the western North Pacific and its adjacent seas. *Marine Chemistry*, *173*, 330–341. https://doi.org/10.1016/j.marchem.2014.10.016

Kim, T., Obata, H., Nishioka, J., & Gamo, T. (2017). Distribution of dissolved zinc in the western and central subarctic North Pacific. *Global Biogeochemical Cycles*, *31*, 1454–1468. https://doi.org/10.1002/2017gb005711

Köbberich, M., & Vance, D. (2017). Kinetic control on Zn isotope signatures recorded in marine diatoms. *Geochimica et Cosmochimica Acta*, *210*, 97–113. https://doi.org/10.1016/j.gca.2017.04.014

Köbberich, M., & Vance, D. (2018). Zinc association with surface-bound iron-hydroxides on cultured marine diatoms: A zinc stable isotope perspective. *Marine Chemistry*, *202*, 1–11. https://doi.org/10.1016/j.marchem.2018.01.002

Köbberich, M., & Vance, D. (2019). Zn isotope fractionation during uptake into marine phytoplankton: Implications for oceanic zinc isotopes. *Chemical Geology*, *523*, 154–161. https://doi.org/10.1016/j.chemgeo.2019.04.004

Lane, E. S., Jang, K., Cullen, J. T., & Maldonado, M. T. (2008). The interaction between inorganic iron and cadmium uptake in the marine diatom Thalassiosira oceanica. *Limnology and Oceanography*, *53*(5), 1784–1789. https://doi.org/10.4319/lo.2008.53.5.1784

Lane, E. S., Semeniuk, D. M., Strzepek, R. F., Cullen, J. T., & Maldonado, M. T. (2009). Effects of iron limitation on intracellular cadmium of cultured phytoplankton: Implications for surface dissolved cadmium to phosphate ratios. *Marine Chemistry*, *115*(3-4), 155–162. https://doi.org/10.1016/j.marchem.2009.07.008

Liao, W.-H., & Ho, T.-Y. (2018). Particulate trace metal composition and sources in the Kuroshio adjacent to the East China Sea: The importance of aerosol deposition. *Journal of Geophysical Research: Oceans*, *123*, 6207–6223. https://doi.org/10.1029/2018jc014113

Liao, W.-H., Yang, S.-C., & Ho, T.-Y. (2017). Trace metal composition of size-fractionated plankton in the Western Philippine Sea: The impact of anthropogenic aerosol deposition. *Limnology and Oceanography*, *62*(5), 2243–2259. https://doi.org/10.1002/lno.10564

Little, S. H., Vance, D., McManus, J., & Severmann, S. (2016). Key role of continental margin sediments in the oceanic mass balance of Zn and Zn isotopes. *Geology*, *44*(3), 207–210. https://doi.org/10.1130/g37493.1

Liu, Z., & Gan, J. (2017). Three-dimensional pathways of water masses in the South China Sea: A modeling study. *Journal of Geophysical Research: Oceans*, *122*, 6039–6054. https://doi.org/10.1002/2016jc012511

Lohan, M. C., Statham, P. J., & Crawford, D. W. (2002). Total dissolved zinc in the upper water column of the subarctic North East Pacific. *Deep Sea Research Part II: Topical Studies in Oceanography*, *49*(24-25), 5793–5808. https://doi.org/10.1016/s0967-0645(02)00215-1

Mahowald, N. M., Engelstaedter, S., Luo, C., Sealy, A., Artaxo, P., Benitez-Nelson, C., et al. (2009). Atmospheric iron deposition: Global distribution, variability, and human perturbations. *Annual Review of Marine Science*, *1*, 245–278. https://doi.org/10.1146/annurev.marine.010908.163727

Marković, T., Manzoor, S., Humphreys-Williams, E., Kirk, G. J. D., Vilar, R., & Weiss, D. J. (2017). Experimental determination of zinc isotope fractionation in complexes with the phytosiderophore 2′-deoxymugeneic acid (DMA) and its structural analogues, and implications for plant uptake mechanisms. *Environmental Science & Technology*, *51*(1), 98–107. https://doi.org/10.1021/acs.est.6b00566

Martin, J. H., Gordon, R. M., Fitzwater, S., & Broenkow, W. W. (1989). Vertex: Phytoplankton/iron studies in the Gulf of Alaska. *Deep Sea Research Part A. Oceanographic Research Papers*, *36*(5), 649–680. https://doi.org/10.1016/0198-0149(89)90144-1

Matsumoto, K. (2007). Radiocarbon-based circulation age of the world oceans. *Journal of Geophysical Research*, *112*, C09004. https://doi.org/10.1029/2007jc004095

Middag, R., de Baar, H. J. W., & Bruland, K. W. (2019). The relationships between dissolved zinc and major nutrients phosphate and silicate along the GEOTRACES GA02 transect in the West Atlantic Ocean. *Global Biogeochemical Cycles*, *33*, 63–84. https://doi.org/10.1029/2018gb006034

Moynier, F., Vance, D., Fujii, T., & Savage, P. (2017). The isotope geochemistry of zinc and copper. *Reviews in Mineralogy and Geochemistry*, *82*(1), 543–600. https://doi.org/10.2138/rmg.2017.82.13

Nishioka, J., Nakatsuka, T., Watanabe, Y. W., Yasuda, I., Kuma, K., Ogawa, H., et al. (2013). Intensive mixing along an island chain controls oceanic biogeochemical cycles. *Global Biogeochemical Cycles*, *27*, 920–929. https://doi.org/10.1002/gbc.20088

Nishioka, J., Ono, T., Saito, H., Nakatsuka, T., Takeda, S., Yoshimura, T., et al. (2007). Iron supply to the western subarctic Pacific: Importance of iron export from the Sea of Okhotsk. *Journal of Geophysical Research*, *112*, C10012. https://doi.org/10.1029/2006jc004055

Nriagu, J. O., & Pacyna, J. M. (1988). Quantitative assessment of worldwide contamination of air, water and soils by trace metals. *Nature*, *333*(6169), 134–139. https://doi.org/10.1038/333134a0

Ohnemus, D. C., Rauschenberg, S., Cutter, G. A., Fitzsimmons, J. N., Sherrell, R. M., & Twining, B. S. (2017). Elevated trace metal content of prokaryotic communities associated with marine oxygen deficient zones. *Limnology and Oceanography*, *62*(1), 3–25. https://doi.org/10.1002/lno.10363

Pacyna, J. M., & Pacyna, E. G. (2001). An assessment of global and regional emissions of trace metals to the atmosphere from anthropogenic sources worldwide. *Environmental Reviews*, *9*(4), 269–298. https://doi.org/10.1139/a01-012

Primeau, F. W., & Holzer, M. (2006). The ocean's memory of the atmosphere: Residence-time and ventilation-rate distributions of water masses. *Journal of Physical Oceanography*, *36*(7), 1439–1456. https://doi.org/10.1175/jpo2919.1

Resing, J. A., Sedwick, P. N., German, C. R., Jenkins, W. J., Moffett, J. W., Sohst, B. M., & Tagliabue, A. (2015). Basin-scale transport of hydrothermal dissolved metals across the South Pacific Ocean. *Nature*, *523*(7559), 200–203. https://doi.org/10.1038/nature14577

Ripperger, S., Rehkämper, M., Porcelli, D., & Halliday, A. N. (2007). Cadmium isotope fractionation in seawater—A signature of biological activity. *Earth and Planetary Science Letters*, *261*(3), 670–684. https://doi.org/10.1016/j.epsl.2007.07.034

Rosca, C., Schoenberg, R., Tomlinson, E. L., & Kamber, B. S. (2018). Combined zinc-lead isotope and trace-metal assessment of recent atmospheric pollution sources recorded in Irish peatlands. *Science of the Total Environment*, *658*, 234–249. https://doi.org/10.1016/j.scitotenv.2018.12.049

Roshan, S., DeVries, T., Wu, J., & Chen, G. (2018). The internal cycling of zinc in the ocean. *Global Biogeochemical Cycles*, *32*, 1833–1849. https://doi.org/10.1029/2018GB006045

Rudge, J. F., Reynolds, B. C., & Bourdon, B. (2009). The double spike toolbox. *Chemical Geology*, *265*(3-4), 420–431. https://doi.org/10.1016/j.chemgeo.2009.05.010

Samanta, M., Ellwood, M. J., Sinoir, M., & Hassler, C. S. (2017). Dissolved zinc isotope cycling in the Tasman Sea, SW Pacific Ocean. *Marine Chemistry*, *192*, 1–12. https://doi.org/10.1016/j.marchem.2017.03.004

Samanta, M., Ellwood, M. J., & Strzepek, R. F. (2018). Zinc isotope fractionation by Emiliania huxleyi cultured across a range of free zinc ion concentrations. *Limnology and Oceanography*, *63*(2), 660–671. https://doi.org/10.1002/lno.10658

Shelley, R. U., Landing, W. M., Ussher, S. J., Planquette, H., & Sarthou, G. (2018). Regional trends in the fractional solubility of Fe and other metals from North Atlantic aerosols (GEOTRACES cruises GA01 and GA03) following a two-stage leach. *Biogeosciences*, *15*(8), 2271–2288. https://doi.org/10.5194/bg-15-2271-2018

Sieber, M., Conway, T. M., de Souza, G. F., Hassler, C. S., Ellwood, M. J., & Vance, D. (2019). Cycling of zinc and its isotopes across multiple zones of the Southern Ocean: Insights from the Antarctic Circumnavigation Expedition. *Geochimica et Cosmochimica Acta*, *268*, 310–324. https://doi.org/10.1016/j.gca.2019.09.039

Siebert, C., Nägler, T. F., & Kramers, J. D. (2001). Determination of molybdenum isotope fractionation by double-spike multicollector inductively coupled plasma mass spectrometry. *Geochemistry, Geophysics, Geosystems*, *2*(7). https://doi.org/10.1029/2000gc000124

Sohrin, Y., Urushihara, S., Nakatsuka, S., Kono, T., Higo, E., Minami, T., et al. (2008). Multielemental determination of GEOTRACES key trace metals in seawater by ICPMS after preconcentration using an ethylenediaminetriacetic acid chelating resin. *Analytical Chemistry*, *80*(16), 6267–6273. https://doi.org/10.1021/ac800500f

Takano, S., Tanimizu, M., Hirata, T., Shin, K.-C., Fukami, Y., Suzuki, K., & Sohrin, Y. (2017). A simple and rapid method for isotopic analysis of nickel, copper, and zinc in seawater using chelating extraction and anion exchange. *Analytica Chimica Acta*, *967*(Supplement C), 1–11. https://doi.org/10.1016/j.aca.2017.03.010

Vance, D., de Souza, G. F., Zhao, Y., Cullen, J. T., & Lohan, M. C. (2019). The relationship between zinc, its isotopes, and the major nutrients in the North-East Pacific. *Earth and Planetary Science Letters*, *525*. https://doi.org/10.1016/j.epsl.2019.115748

Vance, D., Little, S. H., de Souza, G. F., Khatiwala, S., Lohan, M. C., & Middag, R. (2017). Silicon and zinc biogeochemical cycles coupled through the Southern Ocean. *Nature Geoscience*, *10*(3), 202–206. https://doi.org/10.1038/ngeo2890

Wang, B. S., Lee, C. P., & Ho, T. Y. (2014). Trace metal determination in natural waters by automated solid phase extraction system and ICP-MS: The influence of low level Mg and Ca. *Talanta*, *128*, 337–344. https://doi.org/10.1016/j.talanta.2014.04.077

Wang, R. M., Archer, C., Bowie, A. R., & Vance, D. (2019). Zinc and nickel isotopes in seawater from the Indian Sector of the Southern Ocean: The impact of natural iron fertilization versus Southern Ocean hydrography and biogeochemistry. *Chemical Geology*, *511*, 452–464. https://doi.org/10.1016/j.chemgeo.2018.09.010

Watanabe, Y. W., Ishida, A., Tamaki, M., Okuda, K., & Fukasawa, M. (1997). Water column inventories of chlorofluorocarbons and production rate of intermediate water in the North Pacific. *Deep Sea Research Part I: Oceanographic Research Papers*, *44*(7), 1091–1104. https://doi.org/10.1016/s0967-0637(97)00017-4

Weber, T., John, S., Tagliabue, A., & DeVries, T. (2018). Biological uptake and reversible scavenging of zinc in the global ocean. *Science*, *361*(6397), 72–76. https://doi.org/10.1126/science.aap8532

Westerlund, S. F. G., Anderson, L. G., Hall, P. O. J., Iverfeldt, Å., Van Der Loeff, M. M. R., & Sundby, B. (1986). Benthic fluxes of cadmium, copper, nickel, zinc and lead in the coastal environment. *Geochimica et Cosmochimica Acta*, *50*(6), 1289–1296. https://doi.org/10.1016/0016-7037(86)90412-6

Weyer, S., & Schwieters, J. B. (2003). High precision Fe isotope measurements with high mass resolution MC-ICPMS. *International Journal of Mass Spectrometry*, *226*(3), 355–368. https://doi.org/10.1016/s1387-3806(03)00078-2

Xie, R. C., Galer, S. J. G., Abouchami, W., Rijkenberg, M. J. A., de Baar, H. J. W., De Jong, J., & Andreae, M. O. (2017). Non-Rayleigh control of upper-ocean Cd isotope fractionation in the western South Atlantic. *Earth and Planetary Science Letters*, *471*(Supplement C), 94–103. https://doi.org/10.1016/j.epsl.2017.04.024

Yang, L., Nadeau, K., Meija, J., Grinberg, P., Pagliano, E., Ardini, F., et al. (2018). Inter-laboratory study for the certification of trace elements in seawater certified reference materials NASS-7 and CASS-6. *Analytical and Bioanalytical Chemistry*, *410*(18), 4469–4479. https://doi.org/10.1007/s00216-018-1102-y

Yang, S.-C., Lee, D.-C., & Ho, T.-Y. (2012). The isotopic composition of Cadmium in the water column of the South China Sea. *Geochimica et Cosmochimica Acta*, *98*, 66–77. https://doi.org/10.1016/j.gca.2012.09.022

Yang, S.-C., Lee, D.-C., & Ho, T.-Y. (2015). Cd isotopic composition in the suspended and sinking particles of the surface water of the South China Sea: The effects of biotic activities. *Earth and Planetary Science Letters*, *428*, 63–72. https://doi.org/10.1016/j.epsl.2015.07.025

Yang, S.-C., Zhang, J., Sohrin, Y., & Ho, T.-Y. (2018). Cadmium cycling in the water column of the Kuroshio-Oyashio Extension region: Insights from dissolved and particulate isotopic composition. *Geochimica et Cosmochimica Acta*, *233*, 66–80. https://doi.org/10.1016/j.gca.2018.05.001

Zhao, Y., Vance, D., Abouchami, W., & de Baar, H. J. W. (2014). Biogeochemical cycling of zinc and its isotopes in the Southern Ocean. *Geochimica et Cosmochimica Acta*, *125*, 653–672. https://doi.org/10.1016/j.gca.2013.07.045

References From the Supporting Information

Fiedler, P. C., & Talley, L. D. (2006). Hydrography of the eastern tropical Pacific: A review. *Progress in Oceanography*, *69*(2-4), 143–180. https://doi.org/10.1016/j.pocean.2006.03.008

Jakuba, R. W., Saito, M. A., Moffett, J. W., & Xu, Y. (2012). Dissolved zinc in the subarctic North Pacific and Bering Sea: Its distribution, speciation, and importance to primary producers. *Global Biogeochemical Cycles*, *26*, GB2015. https://doi.org/10.1029/2010gb004004

John, S. G. (2012). Optimizing sample and spike concentrations for isotopic analysis by double-spike ICPMS. *Journal of Analytical Atomic Spectrometry*, *27*(12). https://doi.org/10.1039/c2ja30215b

Kim, T., Obata, H., Nishioka, J., & Gamo, T. (2017). Distribution of dissolved zinc in the western and central subarctic North Pacific. *Global Biogeochemical Cycles*, *31*, 1454–1468. https://doi.org/10.1002/2017gb005711

Liu, K.-K., Tseng, C.-M., Wu, C.-R., & Lin, I.-I. (2010). The South China Sea. In K.-K. Liu, et al. (Eds.), *Carbon and nutrient fluxes in continental margins: A global synthesis*, *IGBP book series* (pp. 464–481). Berlin, Germany: Springer.

Mantyla, A. W., & Reid, J. L. (1983). Abyssal characteristics of the World Ocean waters. *Deep Sea Research Part A. Oceanographic Research Papers*, *30*(8), 805–833. https://doi.org/10.1016/0198-0149(83)90002-x

Nitani, H. (1972). Beginning of the Kuroshio. In H. Stommel, & K. Yoshida (Eds.), *Kuroshio—Its physical aspects* (pp. 129–163). Tokyo: Univ. of Tokyo Press.

Pai, S.-C., Jan, S., Chu, K.-S., Huang, P.-Y., & Takahashi, M. M. (2015). Kuroshio or Oyashio -Sources of the 700 m deep ocean water off Hualien coast, eastern Taiwan. *Deep Ocean Water Research*, *15*(3), 107–116.

Schlitzer, R., Anderson, R. F., Dodas, E. M., Lohan, M., Geibert, W., Tagliabue, A., et al. (2018). The GEOTRACES Intermediate Data Product 2017. *Chemical Geology*, *493*, 210–223. https://doi.org/10.1016/j.chemgeo.2018.05.040

Wong, G. T. F., Tseng, C.-M., Wen, L.-S., & Chung, S.-W. (2007). Nutrient dynamics and N-anomaly at the SEATS station. *Deep Sea Research Part II: Topical Studies in Oceanography*, *54*(14-15), 1528–1545. https://doi.org/10.1016/j.dsr2.2007.05.011

Wyatt, N. J., Milne, A., Woodward, E. M. S., Rees, A. P., Browning, T. J., Bouman, H. A., et al. (2014). Biogeochemical cycling of dissolved zinc along the GEOTRACES South Atlantic transect GA10 at 40°S. *Global Biogeochemical Cycles*, *28*, 44–56. https://doi.org/10.1002/2013gb004637

Yasuda, I. (2004). North Pacific Intermediate Water: Progress in SAGE (SubArctic Gyre Experiment) and Related Projects. *Journal of Oceanography*, *60*(2), 385–395. https://doi.org/10.1023/b:Joce.0000038344.25081.42

You, Y., Suginohara, N., Fukasawa, M., Yasuda, I., Kaneko, I., Yoritaka, H., & Kawamiya, M. (2000). Roles of the Okhotsk Sea and Gulf of Alaska in forming the North Pacific Intermediate Water. *Journal of Geophysical Research*, *105*(C2), 3253–3280. https://doi.org/10.1029/1999jc900304